

See discussions, stats, and author profiles for this publication at: <https://www.researchgate.net/publication/267367748>

# Out-of-Plane Flexural Strength of Unreinforced Clay Brick Masonry Walls

Article · September 2007

CITATIONS

70

READS

1,593

2 authors:



**M. C. Griffith**

University of Adelaide

214 PUBLICATIONS 3,323 CITATIONS

[SEE PROFILE](#)



**Jaroslav Vaculik**

University of Adelaide

28 PUBLICATIONS 279 CITATIONS

[SEE PROFILE](#)

Some of the authors of this publication are also working on these related projects:



Seismic Strengthening of Unreinforced Masonry Buildings Using FRP Composites [View project](#)



children's planning [View project](#)

# Out-of-Plane Flexural Strength of Unreinforced Clay Brick Masonry Walls

M.C. Griffith<sup>1</sup> and J. Vaculik<sup>2</sup>

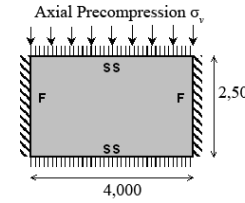
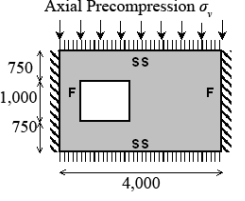
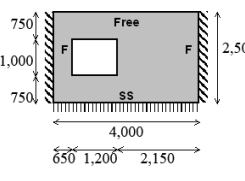
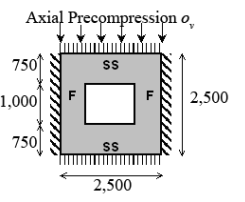
Research into the seismic risk posed by unreinforced masonry (URM) buildings in North America, Europe and New Zealand [Bruneau (1994); Brunsdon (1994); Calvi (1999); Maffei (2000); Abrams (2001)] has highlighted the need for improvements in our understanding of how URM buildings behave under earthquake loading and corresponding improvements in the earthquake design procedures for URM construction. The out-of-plane response of walls is a key aspect of the seismic response of URM buildings.

Significant improvements in the design methods available to calculate the flexural strength of brick masonry walls supported on all four sides and subject to static out-of-plane loads have been achieved [Lawrence and Marshall (2000); Baker, Chen and Drysdale (2005)]. The improvements still assume collapse occurs if a wall's bending strength is exceeded. Typically, this occurs in bending at very small displacements, of the order of 0.1 to 0.2 in. (2 to 5 mm). This may be appropriate for wind loading but it has been shown to be extremely conservative for seismically loaded URM walls [Priestley 1985; Abrams (1996); Magenes and Calvi (1997); Doherty *et al.* (2002)] which do not collapse until the bending displacements approach the thickness of the wall, typically of the order of 4 in. (100 mm) for single leaf clay brick masonry. Some progress has also been made in modelling the non-linear dynamic response of URM buildings [Kelly (1995); Mele (1999); Lourenco (2000)]. However, there is a wide variation in the Young's modulus and tensile and compressive strengths of the masonry. Use of characteristic material strength values (95% lower exclusion values) for limit state strength design, as in the Australian Standard for Masonry Structures (SA 2001), can be very conservative. Hence, work is now underway to extend a newly developed displacement-based procedure for the seismic assessment of URM walls in one-way vertical bending [Doherty *et al.* (2002)] for application to walls in two-way bending. A key step in this development is a better understanding of the full load-deflection behaviour (up to and including collapse) of URM walls in two-way bending.

## EXPERIMENTAL TEST PROGRAM

Eight full-scale unreinforced clay brick masonry walls were subjected to quasi-static displacement-controlled loading as part of this project to investigate the load-deflection behaviour of URM walls beyond their point of maximum strength. The geometry of the eight wall test specimens is given in Table 1 where it can be seen that two solid walls and six walls with openings were considered. Walls 1 and 2 were each 13.12 ft long and 8.20 ft tall (4 m × 2.5 m) and tested with vertical pre-compression of 14.39 psi and 0 psi (0.10 MPa and 0 MPa), respectively. Walls 3 – 5 were also 13.12 ft long by 8.20 feet tall (4 m × 2.5 m) but each wall also had an unsymmetrically

Table 1. Wall Geometry and Boundary Conditions

Wall Geometry and Support Conditions (dimensions in "mm")	Wall	Pre-compression $\sigma_v$
	1	0.10 MPa
	2	0 MPa
	3	0.10 MPa
	4	0.05 MPa
	5	0 MPa
	6	N/A Top edge is unsupported.
	7	0.10 MPa
	8	0 MPa

Note: F = Fixed support, SS = Simple support and 25.4 mm = 1 in.; 1 MPa = 143.9 psi

<sup>1</sup> Associate Professor, Dept of Civil & Env. Eng., University of Adelaide, mcgrif@civeng.adelaide.edu.au

<sup>2</sup> PhD student, Dept of Civil & Env. Eng., University of Adelaide, jvaculik@civeng.adelaide.edu.au

placed window opening located 25.6 in. (650 mm) away from the left-end of the wall. These walls were subject to vertical pre-compression of 14.39 psi, 7.20 psi and 0 psi (0.10 MPa, 0.05 MPa and 0 MPa), respectively. Wall 6 was identical to Wall 5 except that its top edge was free. Walls 7 and 8 were each 8.2 ft by 8.20 ft (2.5 m  $\times$  2.5 m) and had a window opening located symmetrically between each end. A pre-compression of 14.39 psi (0.10 MPa) was also applied to Wall 7.

The walls were constructed by qualified bricklayers using half overlap stretcher bonded masonry with 10-hole cored clay brick units having nominal dimensions for length ( $l_u$ )  $\times$  height ( $h_u$ )  $\times$  width ( $t_u$ ) of 9.06 in.  $\times$  2.99 in.  $\times$  4.33 in. (230 mm  $\times$  76 mm  $\times$  110 mm) and a typical mortar joint thickness ( $t_j$ ) of 0.394 in. (10 mm). The 1:2:9 mortar mix (cement:lime:sand) was bucket batched to minimise mortar batch variability. The engineering properties (mean values and coefficients of variation, CoV) for the brick units and masonry are listed in Table 2 where it can be seen that the quality of the masonry is typical for the mortar mix used. The Young's modulus values for the masonry ( $E_m$ ) and brick units ( $E_u$ ) and the compressive strength of the masonry ( $f_{mc}$ ) were obtained from compression tests on 7 brick tall prisms. The flexural strength of the brick-mortar bond (f<sub>mt</sub>) was determined from bond wrench tests on brick masonry couplets (and/or prisms). The flexural strength of brick units ( $f_{ut}$ ) was determined from simple 4-point bending tests on brick units. All material tests were conducted in accordance with the guidelines given in AS 3700 [SA 2001]).

An important aspect of the experiments was the care taken to simulate simple-supports at the top and bottom edges of the walls and realistic moment connection supports along the vertical edges. Figure 1 illustrates the method used to laterally restrain the top edge of walls, with and without pre-compression. The supports shown in Figure 1 continued along the entire length of the top of each wall. Lateral support was also provided along the entire length of the base of each wall (refer Figure 2) to ensure that the test specimens did not slip at the base.

In order to provide a realistic full moment connection along the vertical edges of each wall, 17.72 in. (450 mm) long return walls were built in as part of each test wall. The return walls were fully engaged through the half-overlap stretcher bonded masonry construction (refer Figure 3). The free end of each return wall was "clamped" by a channel section which was in-turn restrained from moving laterally by bracing back to a support test frame (refer Figure 3b). This enabled the masonry walls to develop their full horizontal bending capacity along the intersection of the main and return walls. An overview of the test set-up for Wall 1 is shown in Figure 4.

Another important focus of these tests was to study the influence of vertical pre-compression on the flexural behaviour of the walls. In order to apply vertical pre-compression to the walls in a realistic manner, a series of steel angle sections were positioned along the test wall at spacings representative of typical roof beam spacings. The angle sections were pinned at one end to a support

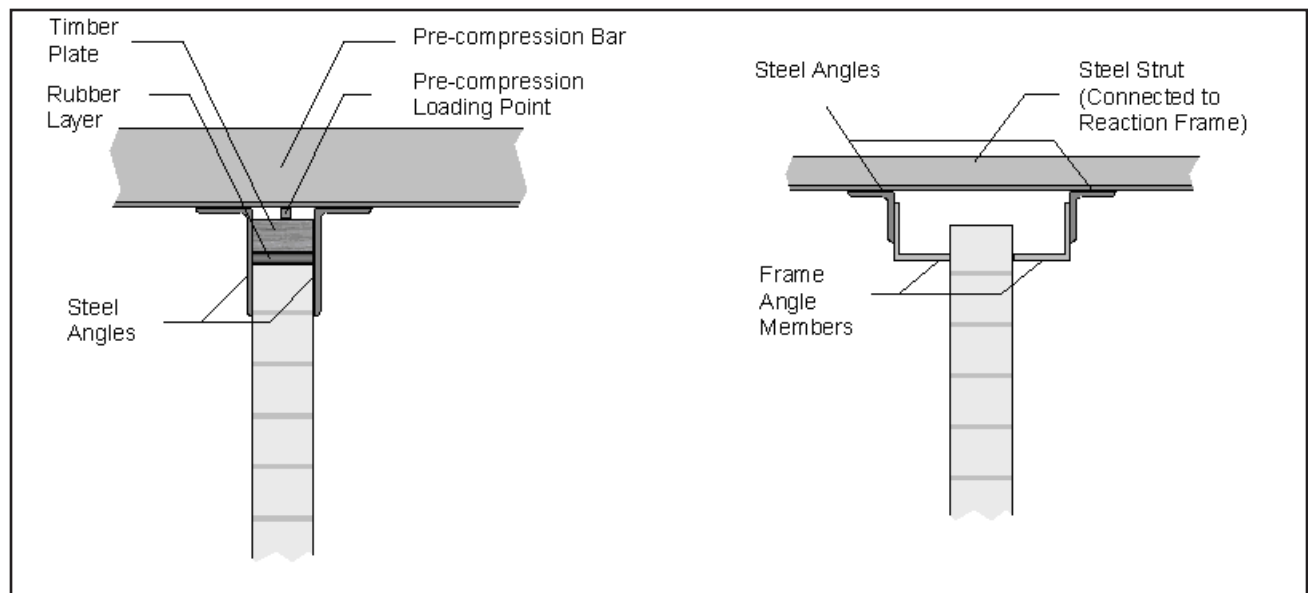
**Table 2. Mean material properties (1 MPa = 143.9 psi)**

<b>(a) Brick Unit Material Properties</b>			
<b>Material Parameter</b>		<b>Mean</b>	<b>CoV</b>
Brick Unit	Lateral modulus of rupture, $f_{ut}$	3.55 MPa	0.27
	Young's modulus, $E_u$	52,700 MPa	0.35

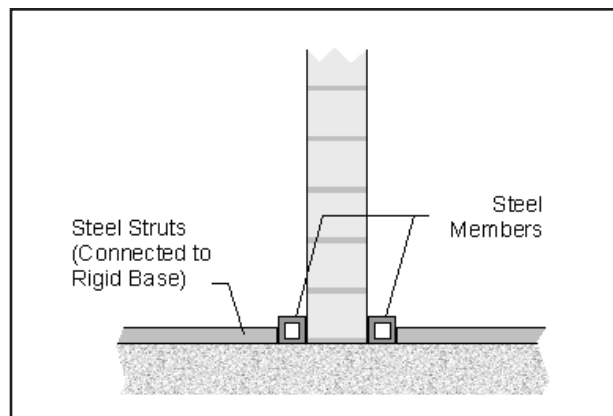
  

<b>(b) Masonry Material Properties</b>			
<b>Wall</b>	<b>Flexural Tensile Strength <math>f_{mt}</math> (MPa)</b>	<b>Compressive Strength <math>f_{mc}</math> (MPa)</b>	<b>Young's Modulus <math>E_m</math> (MPa)</b>
1	0.721	17.6	3,188
2	0.520	13.6	2,240
3	0.499	15.1	3,031
4	0.639	16.8	5,578
5	0.655	17.4	3,991
6	0.496	15.8	2,740
7	0.682	15.1	4,131
8	0.714	16.1	3,057
Mean	0.614	16.0	3,540
CoV	0.19	0.14	0.41

(Note: 1 MPa = 143.9 psi)



**Figure 1—Support details at Top of Wall**



**Figure 2—Support Details Along Bottom Edge of Wall**

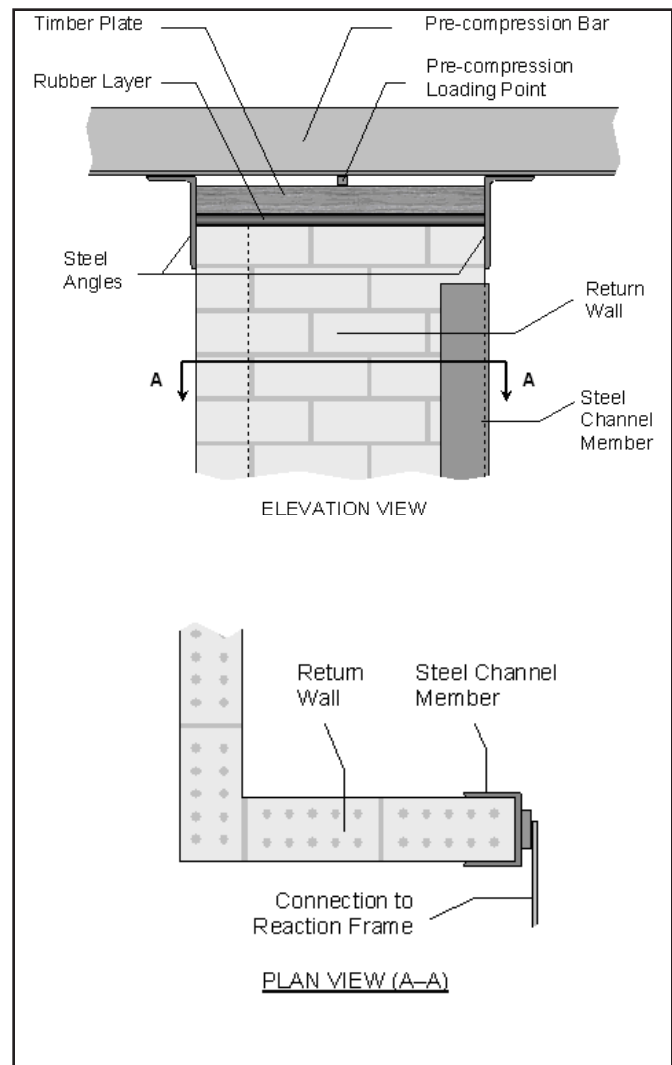


**Figure 3—Support Details Along Vertical Edges of Return Walls**



**Figure 4—Overview of Wall Test Set-Ups**

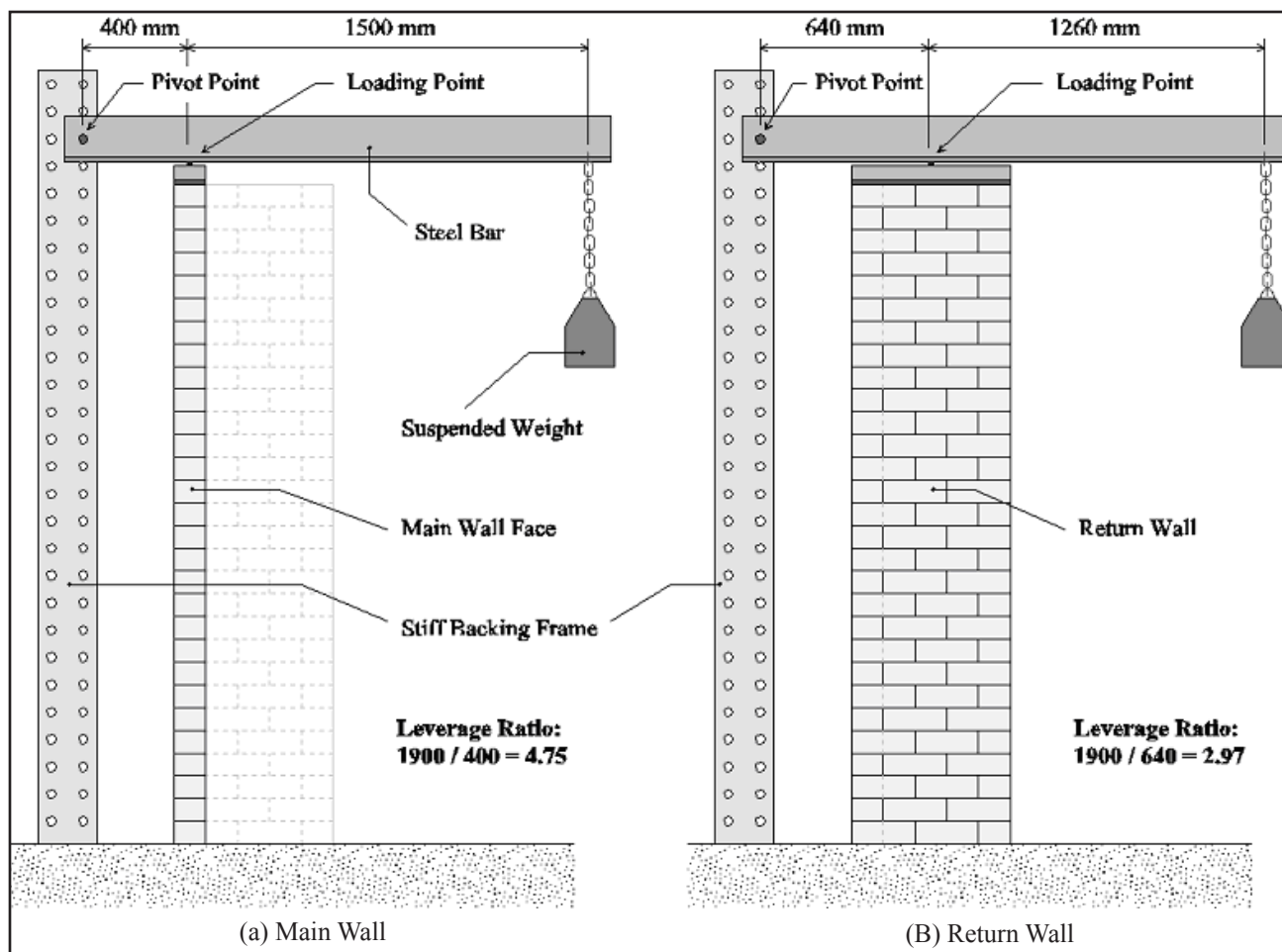


Figure 5—Vertical Pre-Compression Loading Scheme (25.4 mm = 1 in.)

frame (refer Figure 5) and cantilevered over the test wall where it applied a force to the centre of the wall through a loading pin and timber top-plate as shown in Figure 1(a). A lever arm ratio of 4.75 and 2.97 was achieved on the main wall and the return walls, respectively, in order to be able to apply pre-compression stresses of up to 14.39 psi (0.10 MPa) with weights suspended from the end of the angle sections. As indicated in Figure 3(a) and Figure 5(b), the return walls were also loaded with pre-compression to achieve a more uniform stress distribution due to the vertical pre-compression loads. Of course, this had the additional benefit of preventing rigid body overturning of the entire test specimen.

The response of the test walls was monitored with an array of displacement transducers and load cells. The displacement transducer arrangement is shown in Figure 6 where it can be seen that a  $3 \times 3$  grid was used across the wall face to provide a record of the displacement profile for the wall in the horizontal and vertical directions at cross-sections along the walls quarter-span locations. The movement of the walls along their vertical and horizontal edges was also monitored using displacement transducers and where movement along these boundaries took place the measured wall deformations were adjusted accordingly

to produce displacement data for the walls that was in the form of deflections relative to the wall edges.

## TEST RESULTS

The walls were loaded using a system of airbags placed between the wall and a reaction frame. The forces going into the reaction frame were recorded using load cells and these loads, divided by the net surface area for each wall (i.e., wall length  $\times$  height - area of window opening), are plotted against wall deflections for all eight walls in Figures 7 – 9. It should be noted that these plots have duplicated axes at the top and right-hand sides that are in non-dimensional terms where displacement is normalised by the wall thickness,  $t$ , ( $= 110$  mm) and load is normalised by the self-weight of the brickwork,  $\gamma t$ , ( $= 0.301$  psi (2.09 kPa)). The positive deflection direction corresponds to when the applied load pushes the wall inwards and thereby imposes a “compression” reaction onto the return walls. This is also illustrated by the plan view schematic in Figures 7 – 9. The location on the wall for which the deflection was plotted is indicated by a white circle in each figure with the location, in most instances, being the point of maximum deformation in the wall. The specific behaviour of each wall is discussed first before

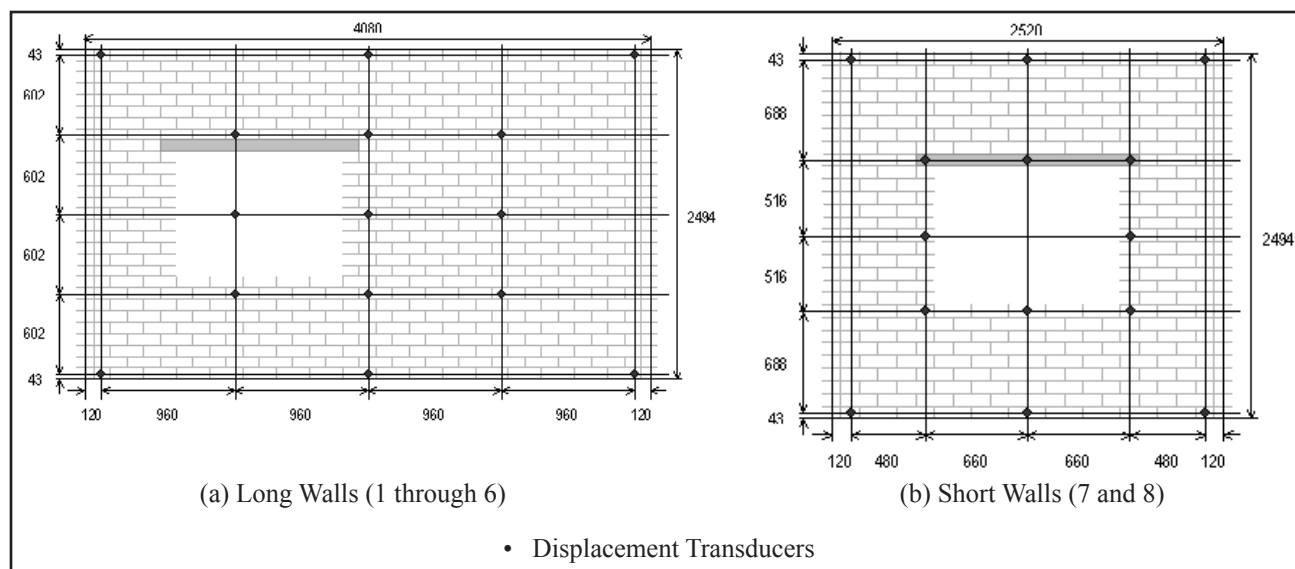


Figure 6—Location of Displacement Transducers (25.4 mm = 1 in.)

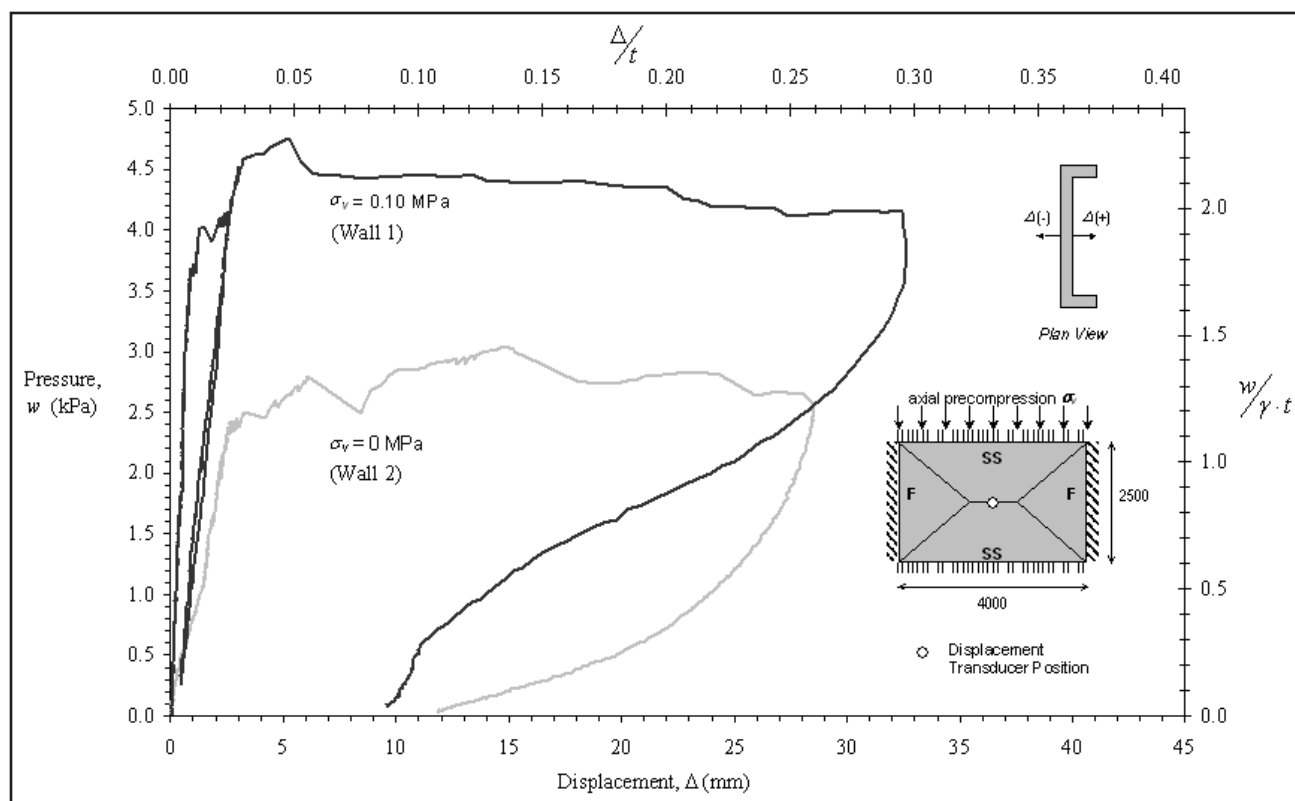


Figure 7—Load-Deflection Response for Long Walls (1 & 2) Without Openings (1 kPa = 0.144 psi and 25.4 mm = 1 in.)

observations are made on the overall trends seen during the experiments.

## Walls 1 & 2

These two solid walls differed only in that wall 2 had no vertical pre-compression ( $\sigma_v = 0$ ). From inspection of the load-deflection response shown in Figure 7, it can be seen that wall 1, with  $\sigma_v = 14.39$  psi (0.1 MPa), was stiffer and stronger. Significantly, both walls displayed

a relatively constant post-peak strength plateau for displacements ranging from 0.1 in. (3 mm) to in excess of 1 in. (25 mm) and this shape is consistent with the generic shape reported by *Lawrence* (1983) for similarly supported walls. The reason for this apparent “plastic” behaviour is believed to be due to redistribution of diagonal bending moment resistance along the diagonal cracks to horizontal bending moment resistance along the vertical edges at the return walls. This observation is further supported by calculations given later in this paper. While both walls



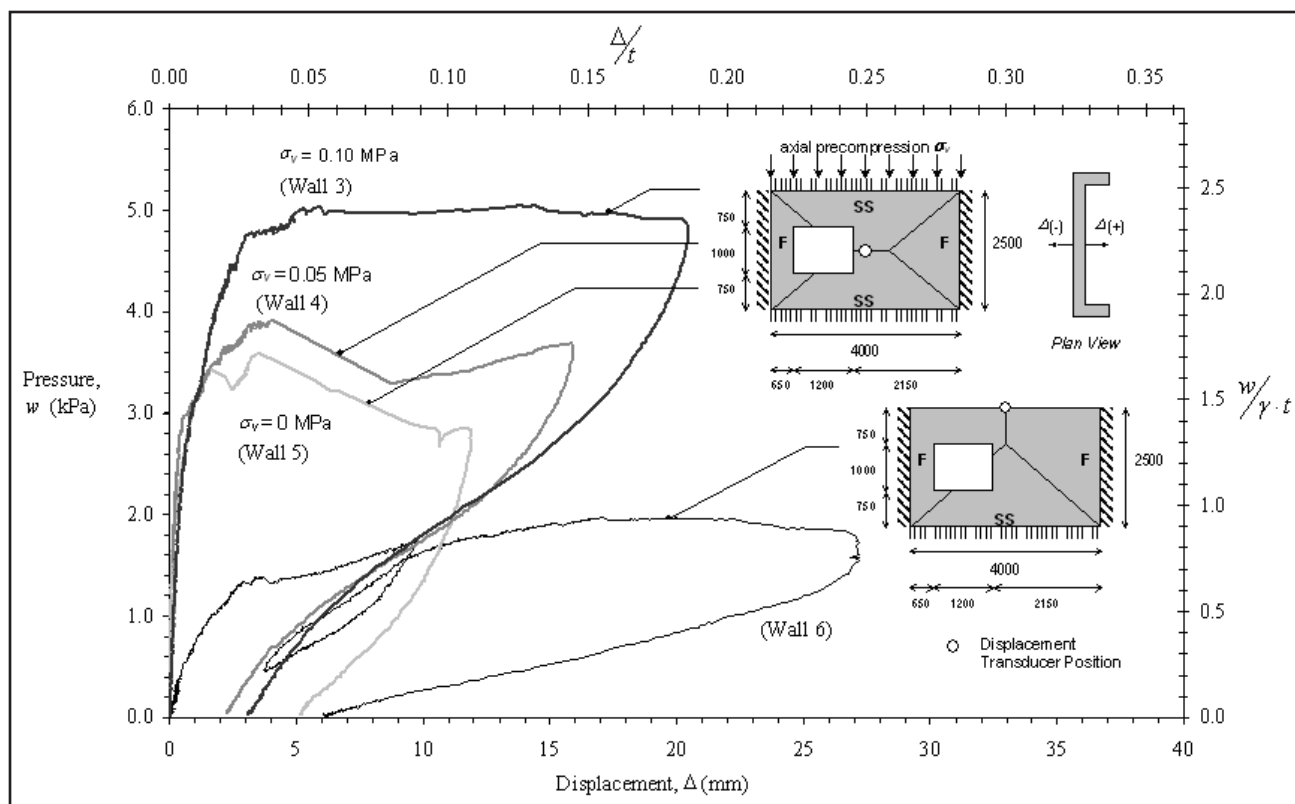


**Figure 8—Load-Displacement Response of Long Walls (3 – 6) with Window Openings**  
(1 kPa = 0.144 psi and 25.4 mm = 1 in.)

unloaded inelastically, wall 1 recovered a larger percentage of its maximum displacement than wall 2, presumably due to its vertical pre-compression load. Wall 1 was also subjected to an unloading cycle before any major cracking had taken place and it can be seen that its response at this early stage of loading was essentially elastic.

The cracking patterns for walls 1 and 2 (Figure 10a,b) also agree well with the idealised cracking patterns shown in Figure 7. Finally, it should be noted that for the walls at this stage of loading, the diagonal cracks were fully developed whereas vertical cracks associated with the horizontal bending mechanism at the vertical edges was only partially developed. This seems to further support the argument that at the point where the full static strength is first reached for these walls, the horizontal bending restraint along the vertical edges has additional capacity to accept transfer of load from the diagonal bending mechanisms.

### Walls 3 - 6

Walls 3 – 6 differed from walls 1 and 2 in that they contained a window opening that was unsymmetrically located closer to the left-hand return wall. Walls 3 – 5 were simply-supported along their top and bottom edges and had vertical pre-compression loading of 14.39, 7.20 and 0 psi (0.10, 0.05 and 0 MPa), respectively. Wall 6 differed from wall 5 only in that its top edge was free.

The load-deflection curves for these walls are shown in Figure 8 where it can be seen again that the walls with more vertical pre-compression were stiffer and stronger. By virtue of its free top edge, wall 6 was much weaker and less stiff than the other three walls.

Significantly, the load-deflection curves for these walls also suggest an apparent “plasticity” over a range of displacements from 0.1 to 0.8 in. (3 to 20 mm) that is also believed to be due to the moment redistribution from moment along the diagonal cracks to the horizontal bending resistance along the vertical edge supports. If one notes the cracking patterns for these walls in Figure 10(c)-(f) it can be seen that they agree reasonably well with the idealised patterns shown in Figure 8. Furthermore, the diagonal cracks are well developed while no vertical cracks were visible at the return wall supports except in wall 3 where they were just starting to appear.

### Walls 7 & 8

Walls 7 and 8 were square with a symmetrically placed window opening and vertical pre-compression loads of 14.39 psi and 0 psi (0.10 MPa and 0 MPa), respectively. As with the other walls, both of these walls displayed a substantial amount of displacement capacity beyond their “elastic limit” and unloaded inelastically (Figure 9). The cracking pattern for wall 7 shown in Fig-

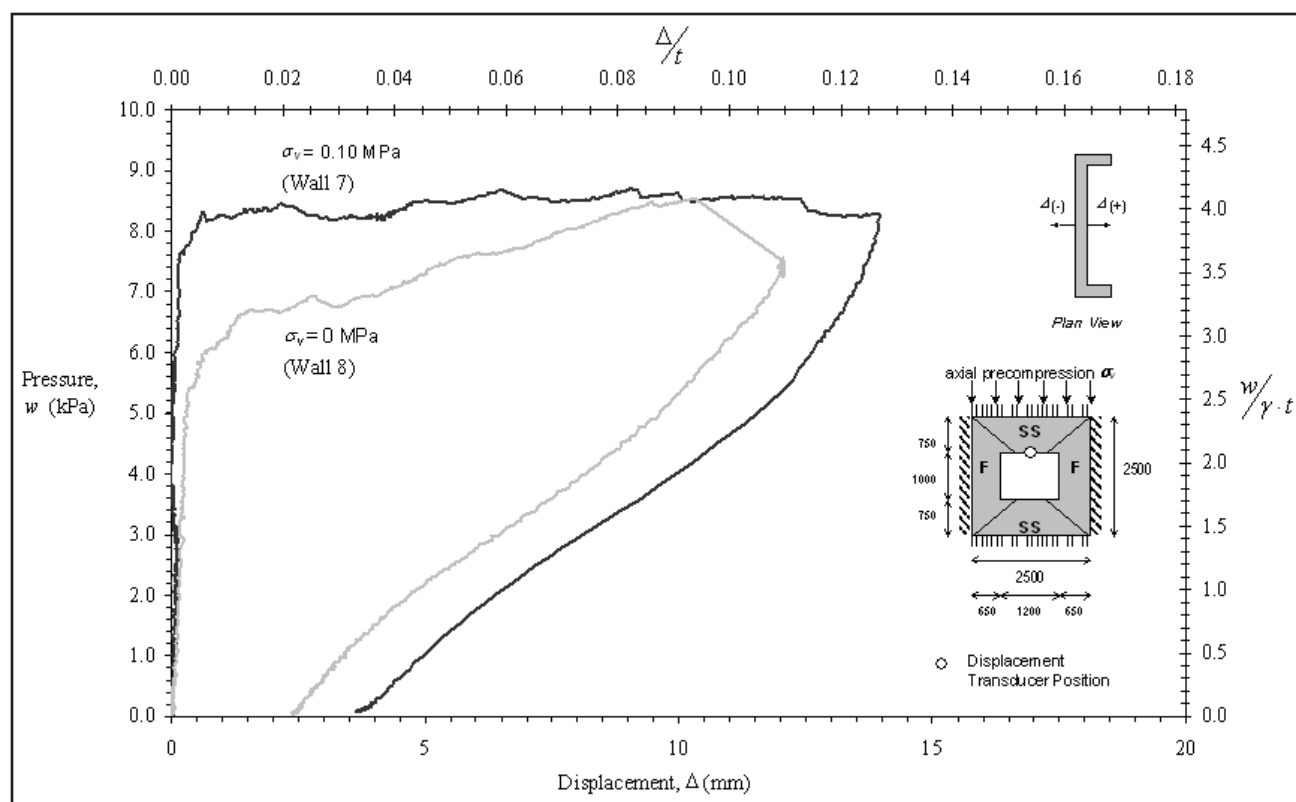


**Figure 9—Load-Deflection Response of Short Walls (7 & 8) with Window Openings**  
(1 kPa = 0.144 psi and 25.4 mm = 1 in.)

ure 10(g) has fully developed diagonal crack lines and a nearly complete vertical crack mechanism in one of the return walls whereas only diagonal cracking is visible for wall 8 in Figure 10(h). This suggests that wall 7 had very nearly developed a full collapse mechanism at which point the strength would be expected to decrease rapidly. Because of the shorter horizontal span, this stage of response was reached at a comparatively small displacement of approximately 0.4 in. (10 mm) whereas the longer walls that were pushed to similar displacements had little or no vertical cracking developed at that displacement.

## General Discussion

The following observations can be made from the load-displacement curves and cracking patterns shown in Figure 7–Figure 10. In every case, there is clear evidence of increased strength and stiffness with increased vertical pre-compression, as shown by comparisons of walls 1 and 2 (Figure 7), walls 3, 4 and 5 (Figure 8) and walls 7 and 8 (Figure 9). This is mainly due to the increased torsional bed joint resistance due to the greater vertical compressive stress on the bed joints, which contributes to the moment capacity of the masonry in both horizontal and diagonal bending.

Significantly, all specimens displayed a more or less constant strength plateau and thus exhibited an apparent ductility and displacement capacity well in excess of the

displacement at which the walls first reached their static strength (typically between 0.08 and 0.2 in. (2 and 5 mm). This behaviour was also noted by *Lawrence* (1983) for tests on 15 walls with similar supports. It should also be pointed out that *Lawrence* (1983) observed no strength plateaus for walls without any rotationally restrained edges. As discussed, it is believed that the constant strength plateau is due to a redistribution of bending moment along diagonal cracks (that develop first) to horizontal bending along the vertical edges. Significantly, good ductility and displacement capacity are highly desirable with respect to earthquake loading.

The walls with openings (3 and 5) had greater strength than the corresponding walls without openings (walls 1 and 2), as shown by Figures 8 and 7, respectively. This counter-intuitive result is due to the fact that the length of diagonal cracks contributing to the wall's resistance (internal work) was mostly unaffected by the presence of a window opening whereas higher pressures were required to generate the corresponding amount of external work because the airbags acted over a reduced area. It should be noted that these tests were intended to simulate inertial loading, such as that due to earthquake, where the distribution of applied load is in direct proportion to the mass distribution of the structure. Because it was deemed that the mass of windows is negligible compared to the mass of the masonry, the openings were not loaded in the test arrangement. Had the walls with openings been subjected



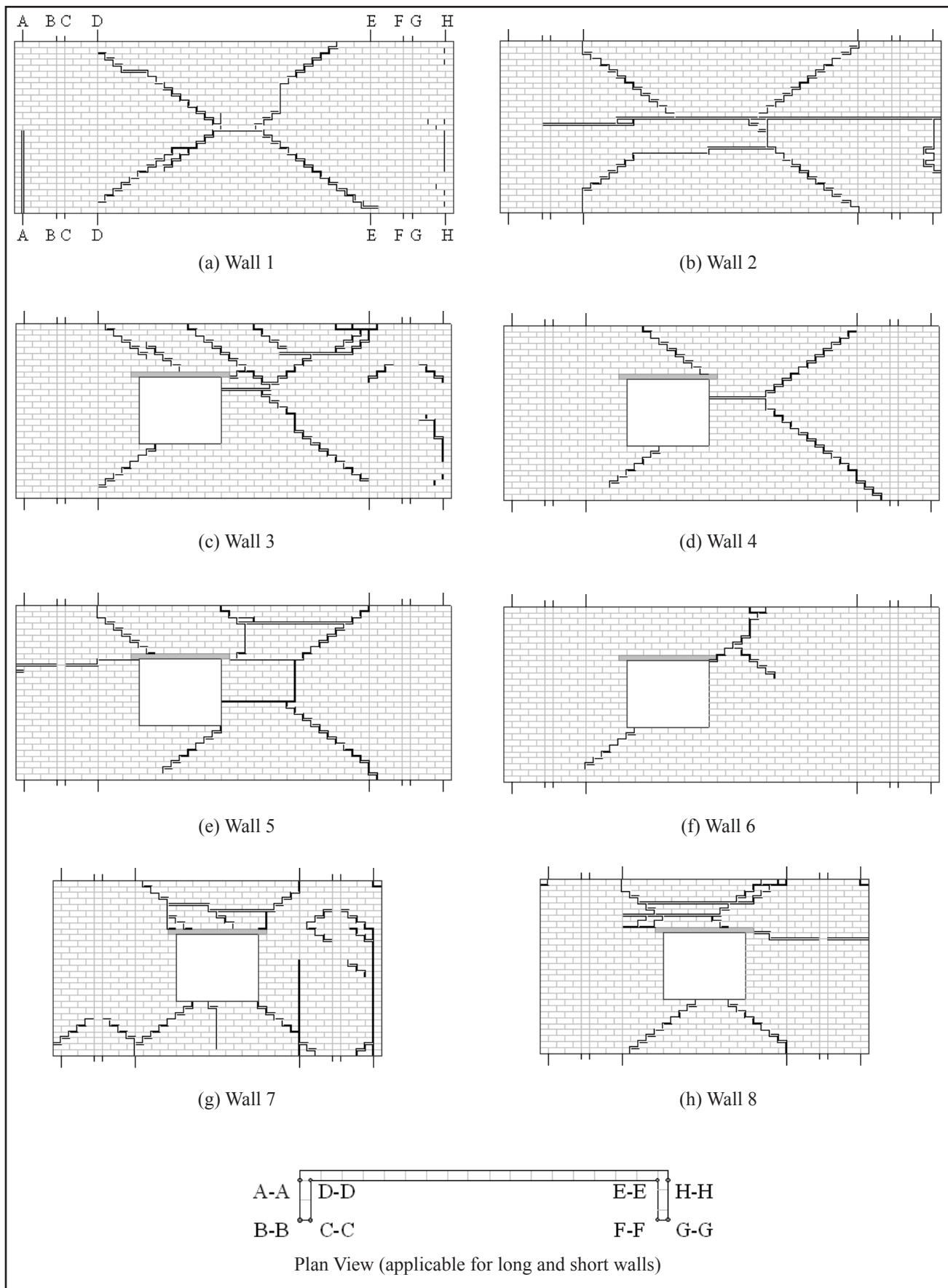


**Figure 10—Cracking Patterns at Conclusion of Static Tests**

to uniform load distribution over their entire face, including openings, the external work done by the loads would be the same as for walls without openings and in that case the presence of openings would be expected to reduce the strength of a wall.

Wall 6 was unsupported at the top edge and exhibited less strength and a significantly larger displacement at the point of ultimate strength compared with the other walls. This is due to wall 6 having a longer effective span and thus requiring a greater central displacement before it could develop the full rotational (i.e., moment) capacity along its vertical edges. In contrast, walls 7 and 8 showed an increase in strength compared with long walls 3 and 5, respectively, due to their shorter horizontal span.

In all cases wall response was highly non-linear and inelastic, resulting in substantial residual deformation. This is indicative of significant energy dissipation capacity – another desirable characteristic with regard to earthquake loading. Interestingly, this result contrasts with the elastic behaviour reported for URM walls in one-way vertical bending [Doherty *et al.* (2002); Meisl *et al.* (2005)] where the mechanism for deflection is primarily rocking about horizontal crack lines.

It can be seen that the idealised cracking patterns (Figures 7 – 9), where the slope of the diagonal cracks is governed by the ratio of the brick unit height to its half length, were in all cases reasonably similar to the observed cracking patterns (Figure 10). All observed cracking patterns were characterised by diagonal cracks propagating from the wall corners where both neighbouring edges were supported. The diagonal cracks did not always follow the idealised slope nor they did not always propagate directly from the corners. However, deviations from the expected behaviour are considered by the authors to be minor. These discrepancies could be attributed to the local variability of material properties, workmanship, and local stress concentrations.

One of the most notable aspects of the crack patterns (Figure 10) is that the walls exhibited only a limited amount of visible cracking at the vertical edges and where present, such cracks were only partially developed. For example, walls 1, 2, 3 and 7 exhibited a limited amount of cracking at the vertical edges whereas walls 4, 5, 6 and 8 showed no visible cracks at these edges at the conclusion of the static test. By contrast, the diagonal cracks were all well developed. This observation suggests that the ultimate moment in horizontal bending along the vertical edges of the walls is achieved at larger wall displacements than that at which the ultimate load capacity in the wall is reached. This issue is further investigated in the analytical discussions in this paper.

## COMPARISON OF IDEALISED AND ACTUAL DISPLACEMENT PROFILES

One of the key assumptions of the method of virtual work, used for predicting the ultimate load capacity of URM walls in the next section of this paper, is that the analysis is based on accurate representation of the actual cracking patterns and corresponding deflected shapes. The accuracy of this assumption is investigated in this section of the paper by comparing the measured displacement profiles along the face of the wall with the displacement profiles corresponding to the idealised failure mechanisms shown in Figures 11 – 14 where, as noted previously, the slope of the diagonal cracks is governed by the ratio of the brick unit height to its half length.

For the eight walls tested, displacement profiles along vertical slices A-A, B-B and C-C (as shown in Figure 11) were determined by calculating each point's deflection relative to the wall boundaries, which were further normalised with respect to the largest relative deflections along the wall face. The resulting plots (Figures 11 – 14), also show the displaced shapes predicted by the idealised collapse mechanisms for comparison. Note that for brevity, the displacement profiles are shown only for selected walls, although these figures are typical of the various categories of walls tested and convey the general trends.

Displacement profiles representative of the two long solid walls are shown by Figure 11 at (a) the point of peak load and (b) at the point of maximum displacement applied to the wall during the static test. It can be seen that the displaced shape is quite symmetric, with the displacements at slice A-A being very comparable to the displacements at slice C-C. Further, the displacement profiles at slices A-A and C-C match reasonably well with the displacements predicted by the idealised shape. The displaced shape along central slice B-B is in very good agreement with the idealised shape, being nearly linear above and below the mid-height crack, especially at the point of maximum displacement (Figure 11b).

It was observed that, in general, the experimentally measured displaced shapes were reasonably comparable both at the point of peak load and at the point of maximum displacement for all the walls tested, although the profiles at the point of maximum displacement tended to be in slightly better agreement with the idealised shapes. This is believed to be a result of the collapse mechanism being more fully developed at the point of maximum applied displacement. Furthermore it will be noted that that the method of virtual work is intrinsically concerned with predicting the peak load resistance of a wall from which it can be reasoned that the displacement profile at the point of peak load is of primary importance. However, it was observed for most walls that there was only a slight drop-off in the load resistance at the point of maximum applied

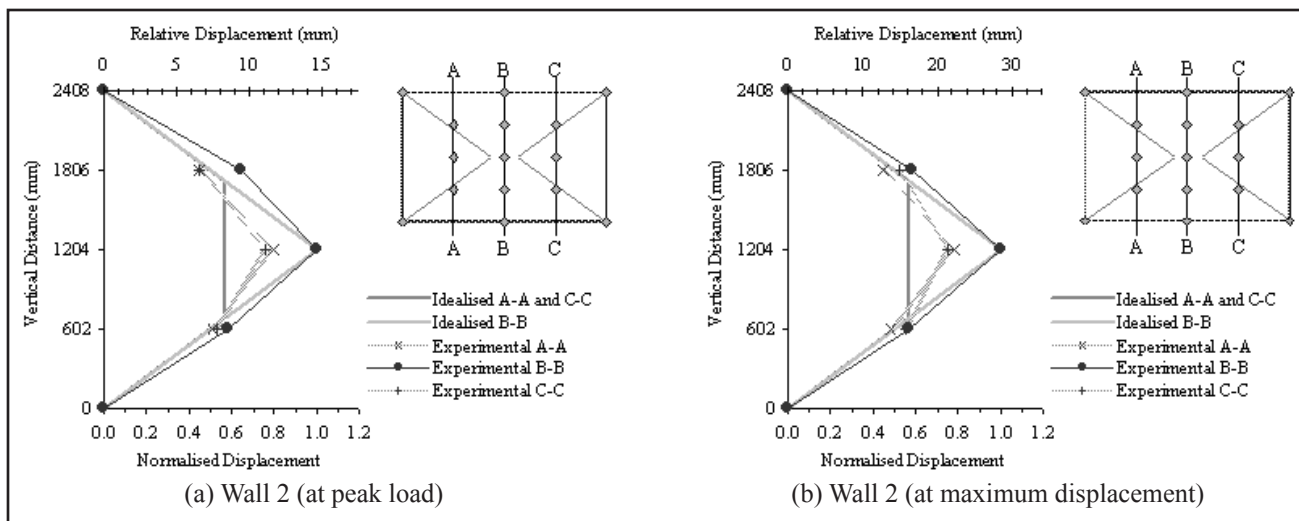


Figure 11—Typical Displacement Profiles for Long Solid Walls (1 – 2) (25.4 mm = 1 in.)

displacement (Figures 7 – 9) so that consideration of the displacement profile at a snapshot anywhere along this 'strength plateau' seems to be quite valid.

Typical displacement profiles for the long walls containing an asymmetric window opening and supported at all four edges (walls 3, 4 and 5) are shown by Figure 12. Asymmetry of the displaced shapes is clearly evident, with displacements at vertical slice C-C exceeding those at slice A-A for each wall in this category. This is believed to be a direct result of the stiffening effect of the lintel located at the top edge of the window opening, in addition to the relative stiffnesses of the local sub-panels at each side of opening. Because the pier to the left of the window opening (as seen from the inside face and shown on Figure 12) has a shorter horizontal span (2.1 ft (0.65 m)) than the pier to the right of the window (7.1 ft (2.15 m)), it is expected to be stiffer and therefore under a uniform

applied pressure undergo a smaller displacement than the less stiff right pier, as indeed indicated by the plots.

In all cases, the experimentally observed displaced shapes of walls 3, 4 and 5 were fairly consistent with the shape of the idealised mechanism, the most notable difference being that the measured displacement at the 1,806 mm (5.925 ft) above the base along section B-B was consistently greater than the displacement predicted by the idealised mechanism. This discrepancy was most pronounced in wall 3 (Figure 12a) where the displacement at the 1,806 mm (5.925 ft) above the base was almost as large as the displacement at the mid-height. This trend suggests that the central horizontal crack formed above the expected mid-height location, as was indeed observed in the crack patterns for all three walls (Figure 10c,d,e). This phenomenon is believed to be a result of the reinforcing action of the lintel, which acted to inhibit propaga-

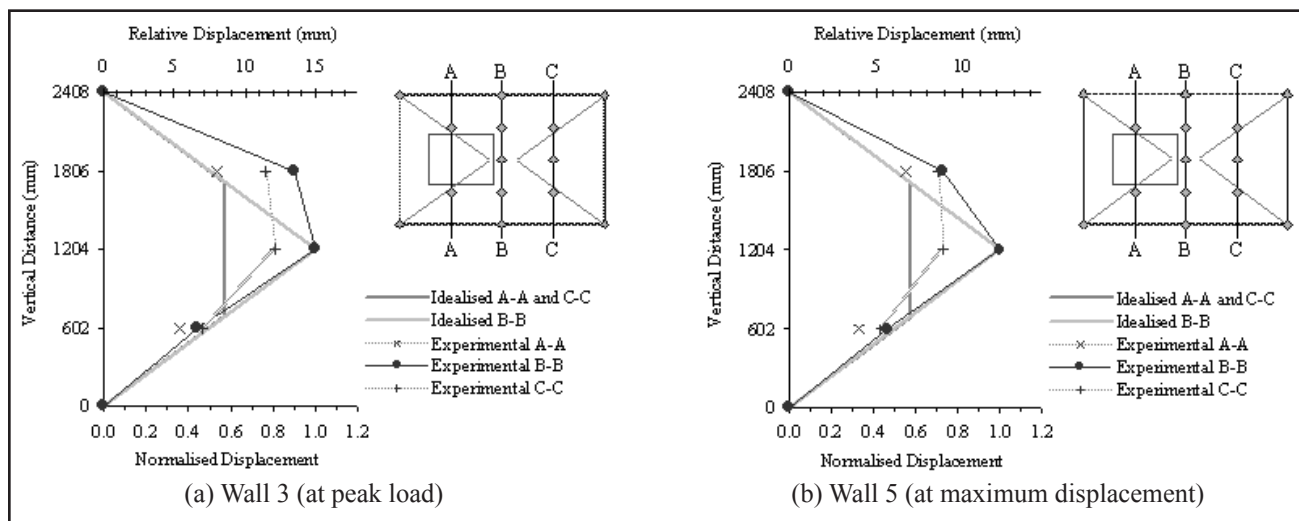
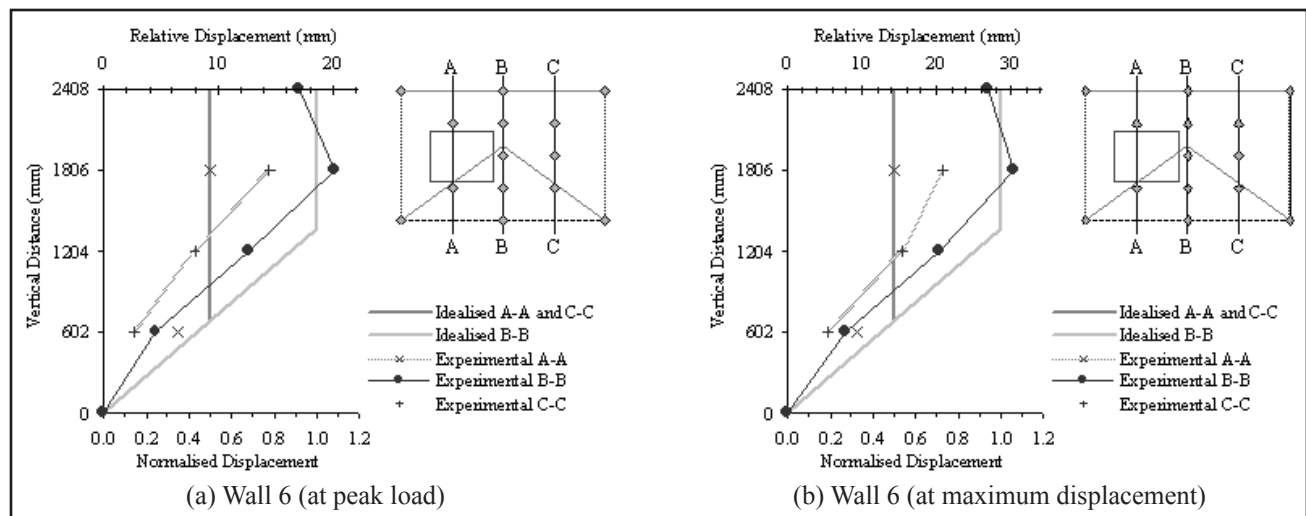


Figure 12—Typical Displacement Profiles for Long Walls (3 – 5) with Asymmetric Opening and Supported at All Four Edges (25.4 mm = 1 in.)



**Figure 13—Displacement Profiles for Long Wall with Asymmetric Opening and Free Top Edge(25.4 mm = 1 in.)**

tion of the top-left diagonal crack and thus promote the formation of a central horizontal crack closer to the top of the wall. Interestingly, the method of virtual work predictions reported in the next section of this paper produced the greatest underestimation of the actual ultimate load for wall 3, in which the aforementioned effect was most pronounced. The authors believe this to be a result of the deviation from the idealised collapse mechanism where the central horizontal crack is at mid-height of the wall, thus minimising the internal work term. Because the central horizontal crack did not actually form at the mid-height, the internal work performed by the wall increased, hence increasing its load resistance.

The displacement profile for the long wall with an asymmetric window opening and free on the top edge (wall 6) is shown in Figure 13. The displaced shapes are comparable at the point of peak load and at maximum displacement and are in good agreement with the shape predicted by the idealised collapse mechanism. While

there is a discrepancy in the ‘slope’ of the displaced shape along slices A-A and C-C, the average displacement at these slices is fairly constant and the overall displaced shape of the wall can be considered to be symmetrical about the central vertical slice B-B. This symmetry is in contrast to the relatively asymmetric profiles observed for walls 3, 4 and 5, which had the same geometry, but were supported at the top edge, and is likely to be a result of the fact that the lintel did not intersect with any of the cracks in neither the observed or idealised failure mechanisms which remained unaltered by its presence.

The displaced shapes of the short walls (7 and 8) containing a centered window opening are shown in Figure 14. It can be seen that the observed displacement profiles suffer from the same discrepancy relative to the idealised displacement profiles, whereby in the observed shapes the displacements along slices A-A and C-C are quite similar in magnitude to the displacements at the central slice B-B, whereas in the idealised shape the displacements at slice B-B should be

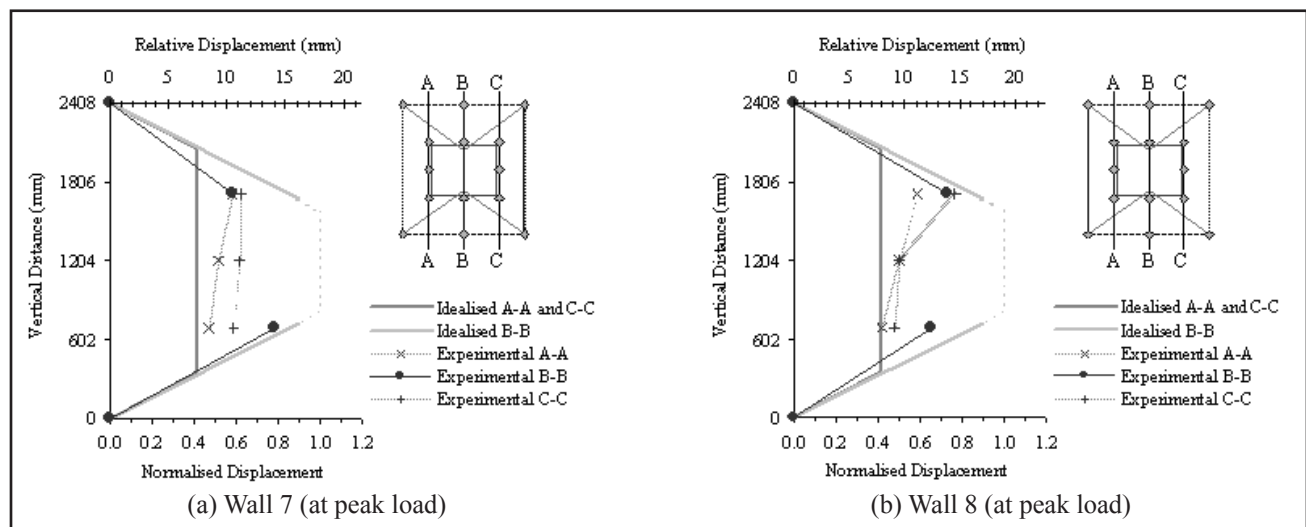


**Figure 14—Displacement Profiles for Short Walls (7 & 8) with Central Opening (25.4 mm = 1 in.)**

significantly greater than the displacements at slices A-A and C-C. This behaviour is believed to result from the stiffening effect of the lintel located at the top edge of the window, which provided a substantial amount of reinforcement in its vicinity the  $3/4$ -height region of the wall, but whose influence also appears to have extended to the  $1/4$ -height region where the measured displacements at the three vertical slices A-A, B-B and C-C were also closely clustered.

## ANALYTICAL PREDICTIONS

In this section the experimental results for the eight walls are compared to the predictions of strength given by applying the principles of virtual work to the idealised failure mechanisms (i.e. cracking patterns) shown in Figures 7 – 9. Note: the virtual work method as described here is similar to the yield line method in that it is an energy-based analytical method. However, the virtual work method differs subtly in that the contributions of vertical bending moment acting along horizontal crack lines is ignored, the slope of diagonal crack lines is governed solely by the brick unit geometry, and moment capacities along vertical and diagonal crack (yield) lines are calculated independently.

The underlying principles state that the work done by the external loads acting on the structure is transformed into an equal amount of internal work or strain energy when the structure deforms. In its application to laterally loaded masonry panels, the external work done on the wall becomes the integral of the applied pressure over the deflected wall shape (Equation 1). The internal work done by the wall is equal to the sum of the internal crack energies at all of the cracks, whereby the crack energy is equal to the product of the moment at the crack line and the rotation of the crack line along its axis (Equation 2).

$$\delta U_{ext} = w \int \delta A dA \quad \text{External Work} \quad (1)$$

$$\delta U_{int} = \sum_{i=1}^n M_i \delta \theta_i \quad \text{Internal Work} \quad (2)$$

Equating the external work to the internal work enables solution for the load resistance of the wall ( $w$ ), as a function of the moment resistance at each crack line ( $M_i$ ) and the displacements ( $\delta A$ ) and rotations ( $\delta \theta$ ) along the wall, which are in turn defined by the failure mechanism. Note,  $M_i$  is the total moment resistance over the full length of crack.

The most important assumptions inherent in the application of this approach are:

- 1) Walls deflect as flat rigid plates bordered by crack lines. This pattern of crack lines defines a collapse mechanism, which the wall exhibits at the point of peak load resistance. The method of virtual work provides an upper-bound estimate of the wall strength, because there exist an infinite

number of possible collapse mechanisms that result in static instability. The critical mechanism is one that occurs under the smallest collapse load;

- 2) Moment capacities along all diagonal and vertical crack lines are reached simultaneously at the point of ultimate strength;
- 3) Horizontal cracks form early in the load-displacement response relative to the point of ultimate strength and thus the moment resistance of these crack lines is assumed to make a negligible contribution to the load resistance and is ignored from the internal work term;

The method of virtual work was used to determine the theoretical strength of the eight tested walls. These analyses utilised the idealised collapse mechanisms shown in Figures 7 – 9, which closely matched the observed cracking patterns shown in Figure 10.

In order to evaluate the internal work, expressions for the horizontal and diagonal bending moment capacity of unreinforced clay brick masonry walls given by Willis *et al.* (2004a, b) were used, as they account for the vertical pre-compression as well as the material properties of the masonry. These expressions, reproduced here for  $M_h$  and  $M_d$ , are the horizontal and diagonal bending moment capacity of the masonry wall per unit length of crack line:

$$M_h = \text{lesser of} \left\{ \begin{array}{l} \frac{1}{2(h_u + t_j)} \left[ (f_{ut} - v \cdot f_d) \cdot h_u \cdot \frac{t_u^2}{6} \right] \\ \frac{1}{h_u + t_j} \left[ \tau_u k_b \cdot 0.5(l_u + t_j) \cdot t_u^2 \right] \end{array} \right. \quad (3a)$$

(3a) Line Failure (3b) Stepped Failure

$$M_d = \frac{\sin \phi}{h_u + t_j} \left[ \frac{(\sin \phi)^3 \tau_u k_b 0.5(l_u + t_j) t_u^2}{+ (\cos \phi)^3 (f_{mt} + f_d) \frac{0.5(l_u + t_j) t_u^2}{6}} \right] \quad (4)$$

where  $l_u$ ,  $t_u$ , and  $h_u$  are, respectively, the length, thickness and height of the brick unit;  $t_j$  is the mortar joint thickness;  $\phi$  is the slope of a diagonal crack line which can be determined from unit geometry;  $f_{mt}$  is the flexural tensile strength of the masonry;  $f_{ut}$  is the flexural tensile strength of the brick unit;  $\tau_u$  is the ultimate shear bond stress of a bed joint given as  $\tau_u = 1.6 f_{mt} + 0.9 f_d$ ;  $v$  is the Poisson's ratio of the masonry, typically taken as 0.2; and  $k_b$  is a numerical factor used to calculate the shear stress due to torque acting on a rectangular cross section [Timoshenko and Goodier (1969)] and is equal to 0.2134 for the half overlap stretcher bonded masonry used in these walls. The term  $f_d$  represents the vertical compressive stress in the wall at its mid-height which includes the vertical pre-compression,  $\sigma_v$ , applied at the top of a wall.

The results of these analytical predictions are given in Table 3 and are, on average 42% greater than the test



values with a coefficient of variation of 0.18. The scatter is illustrated more clearly in Figure 15, where the predictions made using Equations 3 and 4 lie above the line of equality indicating that the method is consistently over-predicting wall strength. This is not surprising, as this application of the virtual work method gives an upper bound prediction of strength, as stated in assumption 1. However, if the assumptions are all valid and the mechanism used in the calculations is correct then the predictions, in principle, should equal the test results. As noted in the previous discussions of the test results, it is believed that the second assumption listed above is not strictly correct. In fact, observations of the sequence of crack formation and the cracking patterns at the conclusion of each test (refer Figure 10) suggest that the moment resistance along the diagonal cracks is reached before the horizontal bend-

ing moment capacity is reached along the vertical edges. Scope is given in the paper by *Lawrence and Marshall* (2000) for treatment of vertical edge supports where the rotational restraint is somewhere between “pinned” and “rigid”. Implicit in the calculations above was an assumption of rotational rigidity along the two vertical edges.

If the virtual work calculations are repeated, but assuming in turn that only half the horizontal bending moment capacity,  $M_h$ , and then none of  $M_h$  is acting along the vertical edges when the wall's full static strength is first attained, modified predictions are given which highlight the sensitivity of the predictions to variations in the first assumption. Table 3 lists the results of these calculations and shows that, on average, by accounting for only half of  $M_h$  at peak wall strength the predictions match very

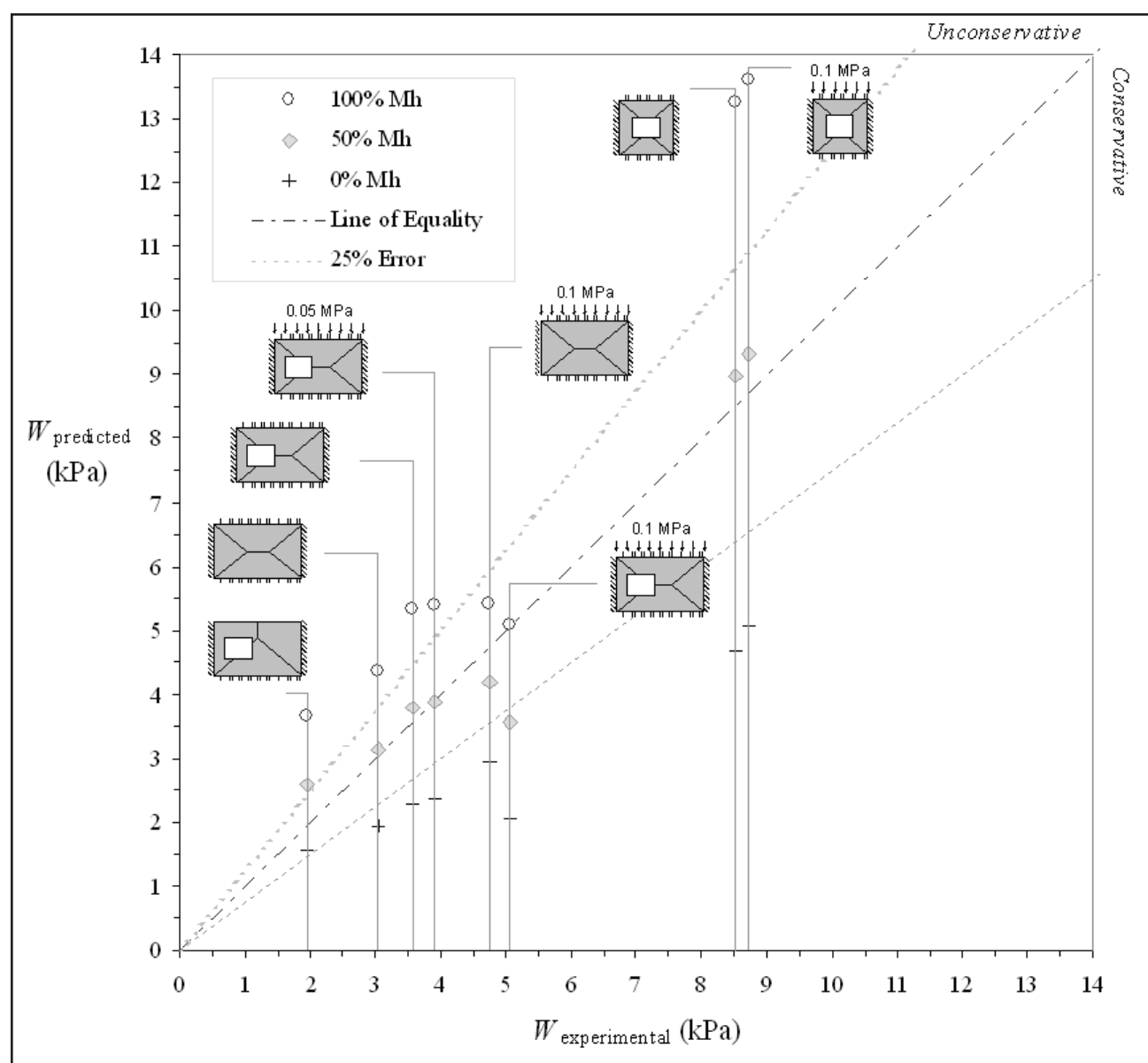


Figure 15—Comparisons of Analytical and Experimental Strength Predictions (1 kPa = 0.1439 psi)



well with the experiment, with only a 1% over-prediction in strength on average. If the contribution of horizontal bending is completely ignored, the predictions are on average 40% below the test results. The authors believe that these calculations further support their conclusion that for walls with vertical edge boundary conditions which are full moment connections but not, strictly speaking, rotationally rigid, it is unlikely that the full moment capacity along diagonal and vertical crack lines will be reached simultaneously. It is their opinion that for the walls in this study the wall attained its peak strength when the diagonal crack lines reached their full moment capacity but at this point, the moment acting at the as-yet uncracked vertical edge supports had not reached its full capacity. The calculations above suggest that the horizontal bending resistance at this point was about 50% of full capacity. Under increasing displacements, the total load applied to the wall remained relatively constant. This was most likely due to a progressive reduction in the moment acting along the diagonal cracks and a compensating increase in the horizontal bending moment acting along the vertical edges. The resulting load-deflection curves are suggestive of wall systems having some “ductility” even though it is recognised that the moment-rotation relationships for local horizontal and diagonal bending,  $M_h$  and  $M_d$ , are elastic-brittle in nature themselves [Willis *et al.* (2004a); Griffith *et al.* (2005)]. The implications of this type of wall behaviour are encouraging from a seismic perspective. Further work is now underway to ascertain if this behaviour is observed under cyclic dynamic loading.

It is of interest that the virtual work method has already been codified [Lawrence and Marshall (2000)] and adopted for use in the Australian Masonry Structures code (SA 2001) after comparison to test results from other researchers (over

60 wall tests) indicated that it generally slightly underestimates wall strength. The main differences between the explicit application of the virtual work method described in this paper and the codified version in AS 3700 is that the code: (1) uses expressions for horizontal and diagonal moment capacity which are empirical, dimensionally inconsistent and which only partially account for the benefits of vertical pre-compression; (2) assumes the load acts over the entire wall face, including the opening, and (3) treats walls with openings using simplified collapse mechanisms, in which the piers on either side of an opening are assumed to act independently. The strength predictions for the wall using the current AS 3700 expressions are given in column 6 of Table 3 (assuming 50% rotational restraint along vertical edges) where it can be seen that they underestimate the experimental strength by 8%, on average. In order to further assess the sensitivity of these calculations to the type of boundary conditions and assumed failure mechanism, a lower bound strip method analysis was performed for each wall. This analysis involved calculating the maximum load that a vertical and horizontal strip of the masonry could resist using the mean material properties in Table 1. The largest of the lower bound estimates was taken to be the critical value. These results are listed in column 7 of Table 3 where it can be seen that these values are, on average, approximately half of the experimental values. This implies a factor of safety of significantly greater than 2 for design where the strip method capacities are calculated using characteristic, rather than mean, material properties.

## SUMMARY AND CLOSING REMARKS

Static airbag tests conducted on eight unreinforced brick masonry walls were described in this paper. All eight walls had full moment connections along both vertical edges

**Table 3. Analytical Predictions by Virtual Work Method (1 kPa = 0.1439 psi)**

Wall	Experimental Ultimate Strength, $w_{exp}$ (kPa)	Ratio of Predicted to Experimental Strength $w_{pred} / w_{exp}$ for Various Analytical Methods				
		Method of Virtual Work			AS 3700 $R_f = 50\%$	Strip Method
		$R_f = 100\%$	$R_f = 50\%$	$R_f = 0$		
1	4.76	1.14	0.88	0.62	1.15	0.46
2	3.04	1.43	1.03	0.64	1.48	0.49
3	5.05	1.00	0.70	0.41	0.60	0.32
4	3.91	1.38	0.99	0.61	0.85	0.47
5	3.59	1.48	1.06	0.64	0.92	0.49
6	1.97	1.85	1.32	0.80	0.72	0.72
7	8.71	1.56	1.07	0.58	0.85	0.45
8	8.52	1.56	1.05	0.55	0.83	0.45
Mean		1.43	1.01	0.60	0.92	0.48
Std Dev		0.26	0.18	0.11	0.27	0.11
CoV		0.18	0.17	0.18	0.30	0.23

and six of the walls also contained a window opening. The experimental data indicates that face-loaded masonry walls have some ductility and a substantial displacement capacity beyond the point of cracking and displacement where the peak strength is first reached. The cracking patterns in the walls at the conclusion of the static tests all agreed reasonably well with the expected cracking patterns with the notable exception that almost no cracking had developed along the vertical edges even though the walls had reached their maximum strength. Further, the deflected shapes for all the walls agreed reasonably well with the idealised shapes corresponding to the assumptions used in the virtual work method. Importantly, the virtual work methodology has been shown to be a potentially useful tool for predicting the static strength of masonry walls in two-way bending. However, these expressions should be used with caution where the vertical edges of walls have full moment connections to the rest of the structure. The results of these tests suggest that only 50% of the horizontal bending capacity is active along the vertical edges of the walls when they first reach their peak strength. Furthermore, walls with longer horizontal span to height ratios would be less influenced by the vertical edge boundary conditions and, as such, would have lower strengths. Nevertheless, the displacement capacity of long walls, where in the limit the response is governed by vertical bending, is typically equal to the wall thickness. The treatment of this condition has been well presented previously by Doherty *et al.* (2002).

## ACKNOWLEDGEMENTS

This research was conducted with the financial support of the Australian Research Council (Grant No. DP0450933) and The University of Adelaide. The technical assistance of staff from the School of Civil and Environmental Engineering is also gratefully acknowledged.

## REFERENCES

- Abrams, D.P., "Performance-based Engineering Concepts for Unreinforced Masonry Building Structures," *Progress in Structural Engineering and Materials*, 3(1): pp. 48-56, 2001.
- Abrams, D.P., Angel, R., Uzarski, J., "Out-of-plane Strength of Unreinforced Masonry Infill Panels," *Earthquake Spectra*, 12(4): pp. 825-844, 1996.
- Baker, C., Chen, B. and Drysdale, R., "Failure Line Method Applied to Walls with Openings," *Proceedings of 10th Canadian Masonry Symposium*, Banff, Alberta, Canada, 2005.
- Bruneau, M., "State-of-the-art Report on Seismic Performance of Unreinforced Masonry Buildings," *ASCE Journal of Structural Engineering*, 120(1): pp. 230-251, 1994.
- Brunsdon, D., "Study Group on Earthquake Risk Buildings 1993/94 Report," *Proceedings of the Technical Conference*, New Zealand Nat. Soc. for Earthquake Eng., pp. 1-6, 1994.
- Calvi, G.M., "A Displacement-based Approach for Vulnerability Evaluation of Classes of Buildings," *Journal of Earthquake Engineering*, 3(3): pp. 411-438, 1999.
- Doherty, K., Griffith, M.C., Lam, N. and Wilson, J., "Displacement-based Analysis for Out-of-Plane Bending of Unreinforced Masonry Walls," *Earthquake Engineering and Structural Dynamics*, John Wiley and Sons, 31(4): pp. 833-850, 2002.
- Griffith, M.C., Magenes, G., Melis, G. and Picchi, L., "Evaluation of Out-of-plane Stability of Unreinforced Masonry Walls Subjected to Seismic Excitation," *Journal of Earthquake Engineering*, Imperial College Press, U.K, 7(1): pp. 141-169, 2003,
- Griffith, M.C., Lawrence, S.J. and Willis, C.R., "Diagonal Bending of Unreinforced Clay Brick Masonry," *Masonry International*, 18(3): pp. 125-138, 2005.
- Kelly, T. "Earthquake Resistant of Unreinforced Masonry Buildings", *Proceedings of the Technical Conference of the New Zealand Nat. Soc. for Earthquake Eng.*, pp. 28-35, 1995.
- Lawrence, S.J., "Behaviour of Brick Masonry Walls Under Lateral Loading," PhD Thesis, The University of New South Wales, 1983.
- Lawrence, S.J. and Marshall, R.J., "Virtual Work Design Method for Masonry Panels under Lateral Load," *Proceedings of the 12th International Brick/Block Masonry Conference*, Madrid, Spain, Vol. 2, pp. 1063-1072, 2000.
- Lourenço, P.B., "Anisotropic Softening Model for Masonry Plates and Shells," *ASCE Journal of Structural Engineering*, 126(9): pp. 1,008-1,016, 2000.
- Maffei, J., Comartin, C.D., Kehoe, B., Kingsley, G.R. and Lizundia, B.C., "Evaluation of Earthquake Damaged Concrete and Masonry Wall Buildings," *Earthquake Spectra*, 16(1) pp. 263-283, 2000.
- Magenes, G. and Calvi, G.M., "In-plane Seismic Response of Brick Masonry Walls", *Earthquake Engineering and Structural Dynamics*, 26(11): pp. 1091-1112, 1997.
- Meisl, C., Mattman, D., Elwood, K., White, T. and Ventura, C., "Out-of-plane Seismic Performance of Unreinforced Clay Brick Masonry Walls," *Proceedings of 10th Canadian Masonry Symposium*, Banff, Alberta, Canada, 2005.

Mele, E., Giordano, A. and De Luca, A., “Nonlinear Analysis of some Typical Elements of a Basilica Plan Church,” *Advances in Earthquake Engineering*, Vol.4, *Earthquake Resistant Engineering Structures II*, WIT Press, Southampton, pp. 533-542, 1999.

Priestley, M. J. N., “Seismic Behaviour of Unreinforced Masonry Walls,” *Bulletin of the New Zealand National Society for Earthquake Engineering*, 18(2): pp. 191-205, 1985.

Standards Australia, “AS 3700 – Masonry Structures,” Standards Association of Australia, Homebush NSW, 2001.

Timoshenko, S. P., and Goodier, J. N. “Theory of Elasticity,” McGraw-Hill, New York, 1969.

Willis, C.R., Griffith, M.C. and Lawrence, S.J., “Horizontal Bending of Unreinforced Clay Brick Masonry Walls,” *Masonry International*, 17(3): pp. 109-121, 2004a.

Willis, C. R., Griffith, M. C. and Lawrence, S. J., “Implications of Recent Experimental and Analytical Studies for the Design of Face-loaded URM Walls,” *Proceedings of the 7th Australasian Masonry Conference*, Newcastle, pp. 255-264, 2004b.

## NOTATION

CoV	=	coefficient of variation.
$E_m$	=	Young’s modulus of masonry.
$E_u$	=	Young’s modulus of brick units.
$f_d$	=	vertical compressive stress in the wall at its mid-height.
$f_{mc}$	=	compressive strength of masonry.
$f_{mt}$	=	flexural tensile strength of brick-mortar bond.
$f_{ut}$	=	lateral modulus of rupture of brick units.
$h_u$	=	height of brick unit.
$k_b$	=	numerical factor used to calculate the shear stress due to torque acting on a rectangular cross section.
$l_u$	=	length of brick unit.
$M_d$	=	diagonal bending moment capacity of masonry.
$M_h$	=	horizontal bending moment capacity of masonry.
$t_j$	=	thickness of mortar joint.
$t_u$	=	thickness of brick unit.
$w$	=	out of plane pressure on masonry wall.
$\gamma$	=	weight density of masonry (weight/volume).
$\nu$	=	Poisson’s ratio of masonry.
$\sigma_v$	=	vertical pre-compression stress.
$\tau_u$	=	ultimate shear bond stress of a bed joint.
$\phi$	=	the slope of a diagonal crack line.